RᴇLAX: Reinforcement Learning Agent Explainer for Arbitrary Predictive Models

Ziheng Chen*
Stony Brook University, USA
ziheng.chen@stonybrook.edu

Fabrizio Silvestri
Sapienza University of Rome, Italy
fsilvestri@diag.uniroma1.it

Jia Wang
The Xi'an Jiaotong-Liverpool
University, China
jia.wang02@xjtlu.edu.cn

He Zhu
Rutgers University, USA
hz375@cs.rutgers.edu

Hongshik Ahn
Stony Brook University, USA
hongshik.ahn@stonybrook.edu

Gabriele Tolomei
Sapienza University of Rome, Italy
tolomei@di.uniroma1.it

ABSTRACT

Counterfactual examples (CFs) are one of the most popular methods for attaching post-hoc explanations to machine learning (ML) models. However, existing CF generation methods either exploit the internals of specific models or depend on each sample's neighborhood, thus they are hard to generalize for complex models and inefficient for large datasets. This work aims to overcome these limitations and introduces RᴇLAX, a model-agnostic algorithm to generate optimal counterfactual explanations. Specifically, we formulate the problem of crafting CFs as a sequential decision-making task and then find the optimal CFs via deep reinforcement learning (DRL) with discrete-continuous hybrid action space. Extensive experiments conducted on several tabular datasets have shown that RᴇLAX outperforms existing CF generation baselines, as it produces sparser counterfactuals, is more scalable to complex target models to explain, and generalizes to both classification and regression tasks. Finally, to demonstrate the usefulness of our method in a real-world use case, we leverage CFs generated by RᴇLAX to suggest *actions* that a country should take to reduce the risk of mortality due to COVID-19. Interestingly enough, the actions recommended by our method correspond to the strategies that many countries have actually implemented to counter the COVID-19 pandemic.

CCS CONCEPTS

• **Computing methodologies** → **Reinforcement learning**; **Sequential decision making**; **Machine learning**; **Artificial intelligence**.

KEYWORDS

machine learning explainability, explainable AI, counterfactual explanations, deep reinforcement learning.

---

*All the authors have contributed equally to this research.

---

1 INTRODUCTION

Recent years have witnessed surprising advances in machine learning (ML), which in turn have led to the pervasive application of ML models across several domains. Unfortunately, though, many ML systems deployed in the wild are treated as "black boxes", whose complexity often hides the inner logic behind their output predictions. In fact, knowing why an ML model returns a certain output in response to a given input is pivotal for a variety of reasons, such as model debugging, aiding decision-making, or fulfilling legal requirements [10].

To properly achieve model transparency, a new initiative named *eXplainable AI* (XAI) has emerged [33]. A large body of work on XAI has flourished in recent years [13], and approaches to XAI can be broadly categorized into two classes [42]: *(i) native* and *(ii) post-hoc.* The former leverages ML models that are inherently interpretable and transparent, such as linear/logistic regression, decision trees, association rules, etc. The latter aims at generating *ex post* explanations for predictions made by opaque or black-box models like random forests and (deep) neural networks.

In this work, we focus on specific post-hoc explanations called *counterfactual explanations*, which are used to interpret predictions of individual instances in the form: "*If A had been different,* B *would not have occurred*" [37][43]. They work by generating modified versions of input samples that result in alternative output responses from the predictive model, i.e., *counterfactual examples* (CFs).

Typically, the problem of generating CFs is formulated as an optimization task, whose goal is to find the "closest" data point to a given instance, which crosses the decision boundary induced by a trained predictive model.[1] Depending on the level of access to the underlying predictive model, different CF generation methods have been proposed. More specifically, we can broadly distinguish between three categories of CF generators: *(i) model-specific* [16–18, 32, 41], *(ii) gradient-aware* [29, 43], and *(iii) model-agnostic* [9]. In short, existing CF generators require complete knowledge of the

---

[1]We voluntarily left this notion of "closeness" underspecified here; a more precise definition of it is provided in Section 3.

model's internals (e.g., random forests or neural networks), or they work only with differentiable models, or finally, they depend on each sample's neighborhood. Thus, they are hard to generalize for more complex models and inefficient for large datasets.

To overcome these limitations, we introduce a novel CF generation method called ReLAX. Specifically, we formulate the problem of crafting CFs as a sequential decision-making task. We then find the optimal CFs via deep reinforcement learning (DRL). The intuition behind ReLAX is the following. The transformation of a given input instance into its optimal CF can be seen as the sequence of actions that an agent must take in order to get the maximum expected reward (i.e., the optimal policy). The total expected reward considers both the desired CF prediction goal (i.e., the CF and the original sample must result in different responses when they are input to the predictive model) and the distance of the generated CF from the original instance. At each time step, the agent has either achieved the desired CF transformation or it needs to: *(i)* select a feature to modify and *(ii)* set the magnitude of such change. To generate meaningful CFs, the agent must restrict itself to operate on the set of *actionable* features only, as not every input feature can always be changed (e.g., the "*age*" of an individual cannot be modified). Moreover, even if actionable, some features can only be changed toward one direction (e.g., a person can only increase their "*educational level*"). Plus, the total number of tweaked features, as well as the magnitude of the change, must also be limited, as this would likely result in a more feasible CF. We show that solving the constrained objective to find the optimal CF generator is equivalent to learning the optimal policy of a DRL agent operating in a discrete-continuous hybrid action space.

Our proposed method is a model-agnostic CF generator, as it can be applied to *any* black-box predictive model. Indeed, in our framework the predictive model is just a "placeholder" resembling the environment which the DRL agent interacts with.

We validate our method on five datasets (four of them used for classification and one for regression), and compare it against several baselines using four standard quality metrics. Experimental results show that ReLAX outperforms all the competitors in every single metric. To further demonstrate the impact of our CF generation method in practice, we show that CFs generated by ReLAX can be leveraged to suggest *actions* that a country should take to reduce the risk of mortality due to the COVID-19 pandemic.

Overall, the main contributions of this work are as follows:

- ReLAX is the first method for generating model-agnostic counterfactual examples based on deep reinforcement learning. It is scalable with respect to the number of features and instances. It can explain *any* black-box model trained on tabular input data, regardless of its internal complexity and prediction task (classification or regression).
- We implement two variants of our method: ReLAX-Global and ReLAX-Local, with the latter obtained via transfer learning from a pretrained version of the former. Both methods generate +60% valid CFs that are about 40% sparser than those produced by state of the art techniques yet take 42% less CF generation time.
- To overcome the sparse reward problem due to the large state and action space, we integrate a hierarchical curiosity-driven exploration mechanism into our DRL agent.

- We further assess the power of ReLAX on a real-world use case. More specifically, we show that the actions suggested by ReLAX to reduce the risk of mortality due to the COVID-19 pandemic correspond to the strategies that many countries have actually put in practice.
- The source code implementation of ReLAX and the datasets (including the one used for the COVID-19 risk of mortality task) are made publicly available.[2]

The remainder of the paper is organized as follows. In Section 2, we review related work. In Section 3, we formalize the problem of generating counterfactual explanations, while in Section 4 we present ReLAX, our proposed method to solve this problem using deep reinforcement learning. We validate our approach and discuss the main findings of our work in Section 5. In Section 6, we further demonstrate the practical impact of ReLAX on a real-world use case. Finally, Section 7 concludes the paper.

2 RELATED WORK

2.1 Counterfactual Explanations for Machine Learning Predictions

A comprehensive review of the most relevant work in this area can be found in [42][12][44][30][23]. A possible approach to counterfactual explanation is called Nearest-CT [20]. Instead of generating a synthetic CF for a given input sample, this approach selects the nearest CF data point from the training set. More sophisticated counterfactual explanation methods can be broadly classified into *model-specific* and *model-agnostic*; as the names suggest, the former are tailored for a particular ML model (e.g., random forest), whereas the latter are able to generate explanations for any model.

Model-specific. One of the first counterfactual explanation method – FeatTweak – is proposed by Tolomei et al. [40], which is specifically designed for random forests, and exploits the internal structure of the learned trees to generate synthetic counterfactual instances. Another approach that is conceived for explaining tree ensembles is called FOCUS [22]. It frames the problem of finding counterfactual explanations as an optimization task and uses probabilistic model approximations in the optimization framework. Meanwhile, the rise of deep learning has given way to more complex and opaque neural networks (NNs). In this regard, DeepFool [27] – which was originally designed for crafting adversarial examples to undermine the robustness of NNs – has proven effective also as a CF generation method. However, CFs obtained from adversarial techniques often require changing almost all the features of the original instances, making them unrealistic to implement. Thus, Le et al. [20] propose GRACE: a novel technique that explains NN model's predictions using sparser CFs, which therefore are suitable also for high-dimensional datasets.

Model-agnostic. Guidotti et al. [13] introduce LORE, which first trains an interpretable surrogate model on a synthetic sample's neighborhood generated by a genetic algorithm. Then, LORE derives an explanation consisting of a decision rule and a set of counterfactual rules. More recently, Karimi et al. [17] propose MACE, which frames the generation of model-agnostic CFs into solving a

---

[2]https://github.com/Mewtwo1996/ReLAX.git

sequence of satisfiability problems, where both the distance function (objective) and predictive model (constraints) are represented as logic formulae. In addition, Mothilal et al. [28] present DiCE, a framework for generating and evaluating a diverse and feasible set of counterfactual explanations, which assumes knowledge of the model's gradients is available, thus not fully model-agnostic.

Our ReLAX method is totally model-agnostic and aims to be as general and flexible as possible. Moreover, different from existing model-agnostic methods, ReLAX is much more efficient to generate optimal CFs. Indeed, ReLAX requires to train a DRL agent that makes use only of the input/output nature of the target predictive model to explain, regardless of its internal complexity or its gradients (as opposed to DiCE). Our method better scales to high-dimensional, large datasets than LORE: the genetic algorithm used to build each synthetic sample's neighborhood may be unfeasible for large feature spaces. Plus, LORE also requires to train a locally-interpretable decision tree that is tight to each generated neighborhood, and therefore may be prone to overfitting. ReLAX can also seamlessly handle more complex models than MACE (e.g., deeper NNs), which needs to construct a first-order logic characteristic formula from the predictive model and test for its satisfiability. This may be intractable when the formula (i.e., the model to explain) is too large. Finally, in contrast with ReLAX, both LORE and MACE do not consider nor control over the sparsity of the generated CFs; moreover, LORE does not even take into account their actionability.

2.2 Reinforcement Learning with Parameterized Action Space

Many real-world reinforcement learning (RL) problems requires complex controls with discrete-continuous hybrid action space. For example, in *Robot Soccer* [25], the agent not only needs to choose whether to shoot or pass the ball (i.e., discrete actions) but also the associated angle and force (i.e., continuous parameters). Unfortunately, most conventional RL algorithms cannot deal with such a heterogeneous action space directly. The straightforward methods either discretize the continuous action space into a large discrete set [35], or convert a discrete action into a continuous action method [14], but they significantly increase the problem complexity. To overcome this issue, a few recent works propose to learn RL policies over the original hybrid action space directly. Specifically, they consider a parameterized action space containing a set of discrete actions $A = \{a_1, a_2, \ldots, a_{|A|}\}$ and corresponding continuous action-parameter $v_k \in V_k \subseteq \mathbb{R}$. In this way, the action space can be represented as: $\mathcal{A} = \bigcup_k \{(a_k, v_k) \mid a_k \in A, v_k \in V_k\}$. Masson et al. [25] propose a learning framework Q-PAMDP that alternatively learns the discrete action selection via Q-learning and employs policy search to get continuous action-parameters. Following the idea of Q-PAMDP, Khamassi et al. [19] treat two actions separately. The only difference is that they use policy gradient to optimize the continuous parameters. Both methods are on-policy and assume that continuous parameters are normally distributed. Also, Wei et al. [45] propose a hierarchical approach to deal with the parameterized action space, where the parameter policy is conditioned on the discrete policy. Although efficient, this method is found to be unstable due to its joint-learning nature. Recently, in order to avoid approximation as well as reduce complexity, Xiong

et al. [49] introduce P-DQN, which seamlessly combines and integrate both DQN [26] and DDPG [21]. Empirical study indicates that P-DQN is efficient and robust.

3 PROBLEM FORMULATION

Let $X \subseteq \mathbb{R}^n$ be an input feature space and $\mathcal{Y}$ an output label space. Without loss of generality, we consider both the K-ary *classification* setting, i.e., $\mathcal{Y} = \{0, \ldots, K-1\}$, and the *regression* setting, i.e., $\mathcal{Y} \subseteq \mathbb{R}$. Suppose there exists a predictive model $h_\omega : X \mapsto \mathcal{Y}$, parameterized by ω, which accurately maps any input feature vector $x = (x_1, \ldots, x_n) \in X$ to its label $h_\omega(x) = y \in \mathcal{Y}$.

The idea of counterfactual explanations is to reveal the rationale behind predictions made by h_ω on individual inputs x by means of counterfactual examples (CFs). More specifically, for an instance x, a CF $\widetilde{x} \neq x$ according to h_ω is found by perturbing a subset of the features of x, chosen from the set $\mathcal{F} \subseteq \{1, \ldots, n\}$. The general goal of such modification is to transform x into $\widetilde{x}$ so to change the original prediction, i.e., $h_\omega(\widetilde{x}) \neq h_\omega(x)$ [43]. In particular, this depends on whether h_ω is a classifier or a regressor. In the former case, the objective would be to transform x into $\widetilde{x}$ so to change the original predicted class $c = h_\omega(x)$ into another $\widetilde{c} = h_\omega(\widetilde{x})$, such that $\widetilde{c} \neq c$. Notice that $\widetilde{c}$ can be either specified upfront (i.e., *targeted* CF) or it can be *any* $\widetilde{c} \neq c$ (i.e., *untargeted* CF). In the case h_ω is a regressor, instead, the goal is trickier: one possible approach to specifying the validity of a counterfactual example $\widetilde{x}$ is to set a threshold $\delta \in \mathbb{R} \setminus \{0\}$ and let $|h_\omega(\widetilde{x}) - h_\omega(x)| \geq \delta$. However, CFs found via such a thresholding are sensitive to the choice of δ [36].

Either way, as long as the CF classification or regression goal is met, several CFs can be generally found for a given input x. This may lead to a situation where many CFs are in fact unrealistic or useless, as they are too far from the original instance. Therefore, amongst all the possible CFs, we search for the *optimal* $\widetilde{x}^*$ as the "closest" one to x. Intuitively, this is to favor CFs that require the *minimal* perturbation of the original input.

More formally, let $g_\theta : X \mapsto X$ be a counterfactual generator, parameterized by θ, that takes as input x and produces as output a counterfactual example $\widetilde{x} = g_\theta(x)$. For a given sample $\mathcal{D}$ of i.i.d. observations drawn from a probability distribution, i.e., $\mathcal{D} \sim p_{\text{data}}(x)$, we can measure the cost of generating CFs with g_θ for all the instances in $\mathcal{D}$, using the following counterfactual loss function:

$$\mathcal{L}_{\text{CF}}(g_\theta; \mathcal{D}, h_\omega) = \frac{1}{|\mathcal{D}|} \sum_{x \in \mathcal{D}} \ell_{\text{pred}}(x, g_\theta(x); h_\omega) + \lambda \ell_{\text{dist}}(x, g_\theta(x)).$$
(1)

The first component (ℓ_{pred}) penalizes when the CF prediction goal is *not* satisfied. Let $C \subseteq X$ be the set of inputs which do *not* meet the CF prediction goal, e.g., in the case of classification, $C = \{x \in X \mid h_\omega(x) = h_\omega(g_\theta(x))\}$. Hence, we can compute ℓ_{pred} as follows:

$$\ell_{\text{pred}}(x, g_\theta(x); h_\omega) = \mathbb{1}_C(x),$$
(2)

where $\mathbb{1}_C(x)$ is the well-known 0-1 indicator function, which evaluates to 1 iff $x \in C$, 0 otherwise.

The second component $\ell_{\text{dist}} : X \times X \mapsto \mathbb{R}_{>0}$ is any arbitrary distance function that discourages $\widetilde{x}$ to be too far away from x. For example, $\ell_{\text{dist}}(x, g_\theta(x)) = ||x - g_\theta(x)||_p$, where $|| \cdot ||_p$ is the L^p-norm. In this work, inspired by previous approaches, we set ℓ_{dist} equal to L^1-norm [13].

In addition, λ serves as a scaling factor to trade off between ℓ_{dist} and ℓ_{pred}. Notice, though, that not every input feature can be lightheartedly modified to generate a valid CF, either because it is strictly impossible to do it (e.g., the "*age*" of an individual cannot be changed), and/or due to ethical concerns (e.g., the "*race*" or the "*political tendency*" of a person). Therefore, we must restrict $\mathcal{F}$ to the set of *actionable* features only. Plus, the total number of perturbed features must also be limited, i.e., $|\mathcal{F}| \leq m$ for some value $1 \leq m \leq n$.

Eventually, we can find the optimal CF generator $g^* = g_{\theta^*}$ as the one whose parameters θ^* minimize Equation 1, i.e., by solving the following constrained objective:

$$\theta^* = \arg\min_{\theta} \left\{ \mathcal{L}_{\text{CF}}(g_\theta; \mathcal{D}, h_\omega) \right\}$$
$$\text{subject to:} \quad |\mathcal{F}| \leq m. \tag{3}$$

This in turn allows us to generate the optimal CF $\widetilde{x}^*$ for any x, as $\widetilde{x}^* = g^*(x)$. Finally, the resulting optimal counterfactual explanation can be simply computed as $e_x = \widetilde{x}^* - x$ [39]. The overview of a generic counterfactual explanation framework is shown in Figure 1.
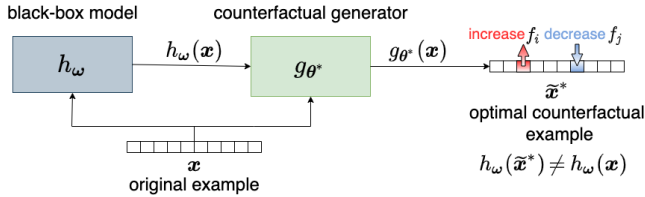

Figure 1: Overview of a generic counterfactual explainer.

4 PROPOSED FRAMEWORK: ReLAX

In this work, we propose to find the optimal CF generator for any arbitrary model – i.e., to solve the constrained optimization problem defined in Equation 3 – via deep reinforcement learning (DRL). We call our method *Reinforcement Learning Agent eXplainer* (ReLAX).

4.1 Markov Decision Process Formulation

We consider the problem of computing the optimal counterfactual example $\widetilde{x}^*$ from $x \in \mathcal{D}$ – i.e., the optimal CF generator g^* defined in Equation 3 – as a sequential decision-making task. More precisely, we refer to the standard reinforcement learning setting, where at each time step an agent: *(i)* takes an action (i.e., selects a feature of the original sample x to tweak *and* the magnitude of such change) and *(ii)* receives an observation (i.e., the prediction output by h_ω on the input just modified according to the action taken before) along with a scalar reward from the environment. The process continues until the agent eventually meets the specified CF prediction goal and the optimal CF $\widetilde{x}^*$ is found.

We formulate this process as a standard Markov Decision Process (MDP) $\mathcal{M} = \{\mathcal{S}, \mathcal{A}, \mathcal{T}, p_0, r, \gamma\}$. In the following, we describe each component of this framework, separately.

4.1.1 States ($\mathcal{S}$). At each time step t, the agent's state is $S_t = s_t$, where $s_t = (x_t, f_t) \in \mathcal{S}$ represents the current modified sample (x_t) along with the set of features changed so far (f_t). More specifically, $f_t \in \{0, 1\}^{|\mathcal{F}|}$ is an $|\mathcal{F}|$-dimensional binary indicator vector,

where $f_t[k] = 1$ iff the actionable feature k has been modified in one of the actions taken by the agent *before* time t. Initially, when $t = 0$, $x_0 = x$ and $f_0 = 0^{|\mathcal{F}|}$.

If the prediction goal is met, e.g., $h_\omega(x_t) \neq h_\omega(x)$, the agent reaches the end of the episode and the process terminates returning $\widetilde{x}^* = x_t$ as the CF for x. Otherwise, the agent must select an action $A_t = a_t$ to: *(i)* pick a feature to change amongst those which have not been modified yet and *(ii)* decide the magnitude of that change.

4.1.2 Discrete-Continuous Hybrid Actions ($\mathcal{A}$). To mimic the two-step behavior discussed above, we consider a discrete-continuous hybrid action space with a two-tier hierarchical structure.

For an arbitrary step t, we maintain the set of feature identifiers that the agent is allowed to modify $\mathcal{F}_t$; initially, when $t = 0$, $\mathcal{F}_0 = \mathcal{F}$ as the agent can pick *any* of the actionable features to change. Then, at each time step $t > 0$, the agent first chooses a high level action k_t from the discrete set $\mathcal{F}_t \subset \mathcal{F} = \mathcal{F} \setminus \bigcup_{j=0}^{t-1} k_j$. This is to allow each feature to be selected at most in one action. Upon choosing $k_t \in \mathcal{F}_t$, the agent must further select a low level parameter $v_{k_t} \in \mathbb{R}$, which specifies the magnitude of the change applied to feature k_t. It is worth noticing that we can confine the action's range and direction by directly putting a constraint on the low level parameter v_{k_t}. Overall, $a_t = (k_t, v_{k_t})$, and we define our discrete-continuous hybrid action space as follows:

$$\mathcal{A}_t = \{(k_t, v_{k_t}) \mid k_t \in \mathcal{F}_t, v_{k_t} \in \mathbb{R}\}.$$

4.1.3 Transition Function ($\mathcal{T}$). Let $a_t = (k_t, v_{k_t}) \in \mathcal{A}_t$ be the generic action that the agent can take at time t. The action a_t deterministically moves the agent from state s_t to state s_{t+1}, by operating on x_t and f_t as follows:

$$\mathcal{T}((x_t, f_t), a_t, (x_{t+1}, f_{t+1})) = \begin{cases} 1, & \text{if } x_t \overset{a_t}{\rightsquigarrow} x_{t+1} \wedge f_t \overset{a_t}{\rightsquigarrow} f_{t+1} \\ 0, & \text{otherwise.} \end{cases} \tag{4}$$

The statements $x_t \overset{a_t}{\rightsquigarrow} x_{t+1}$ and $f_t \overset{a_t}{\rightsquigarrow} f_{t+1}$ are shorthand for $x_{t+1}[k_t] = x_t[k_t] + v_{k_t}$ and $f_{t+1}[k_t] = 1$, respectively. This corresponds to increasing the value of feature k_t by the magnitude v_{k_t}, and updating the binary indicator vector f_t accordingly.

4.1.4 Reward (r). The reward is expressed in terms of the objective function defined in Equation 3 and has the following form:

$$r(s_t, a_t) = \begin{cases} 1 - \lambda(\ell_{\text{dist}}^t - \ell_{\text{dist}}^{t-1}), & \text{if } h_\omega(x_t) \neq h_\omega(x) \\ -\lambda(\ell_{\text{dist}}^t - \ell_{\text{dist}}^{t-1}), & \text{otherwise,} \end{cases} \tag{5}$$

where $\ell_{\text{dist}}^t = \ell_{\text{dist}}(x, x_t)$ and $\lambda \in \mathbb{R}_{>0}$ is a parameter that controls how much weight to put over the distance between the current modified instance (x_t) and the original sample (x). In other words, the agent aims to reach a trade-off between achieving the CF prediction goal and keeping the distance of the counterfactual from the original input sample x as lower as possible.

4.1.5 Policy (π_θ). We define a *parameterized* policy π_θ to maximize the expected reward in the MDP problem. Our ultimate goal, though, is to find an optimal policy $\pi^* = \pi_{\theta^*}$ that solves Equation 3. It is worth noticing that finding the optimal policy π^* that maximizes the expected return in this environment is equivalent to minimizing Equation 1, and thereby finding the optimal CF generator g^*. The

equivalence between these two formulations is shown below:

$$\boldsymbol{\theta}^* = \arg\min_{\boldsymbol{\theta}} \frac{1}{|\mathcal{D}|} \sum_{\boldsymbol{x} \in \mathcal{D}} \ell_{\text{pred}}(\boldsymbol{x}, g_{\boldsymbol{\theta}}(\boldsymbol{x}); h_{\boldsymbol{\omega}}) + \lambda \ell_{\text{dist}}(\boldsymbol{x}, g_{\boldsymbol{\theta}}(\boldsymbol{x}))$$

$$= \arg\max_{\boldsymbol{\theta}} \frac{1}{|\mathcal{D}|} \sum_{\boldsymbol{x} \in \mathcal{D}} -\ell_{\text{pred}}(\boldsymbol{x}, g_{\boldsymbol{\theta}}(\boldsymbol{x}); h_{\boldsymbol{\omega}}) - \lambda \ell_{\text{dist}}(\boldsymbol{x}, g_{\boldsymbol{\theta}}(\boldsymbol{x}))$$

$$= \arg\max_{\boldsymbol{\theta}} \frac{1}{|\mathcal{D}|} \sum_{\boldsymbol{x} \in \mathcal{D}} \begin{cases} 1 - \lambda(\ell_{\text{dist}}^t - \ell_{\text{dist}}^{t-1}), & \text{if } h_{\boldsymbol{\omega}}(\boldsymbol{x}_t) \neq h_{\boldsymbol{\omega}}(\boldsymbol{x}) \\ -\lambda(\ell_{\text{dist}}^t - \ell_{\text{dist}}^{t-1}), & \text{otherwise,} \end{cases}$$

$$= \arg\max_{\boldsymbol{\theta}} \frac{1}{|\mathcal{D}|} \sum_{\boldsymbol{x} \in \mathcal{D}} \sum_{t=1}^{T} r(s_t, \pi_{\boldsymbol{\theta}}(s_t)).$$

Here, T defines the maximum steps taken by the agent for each sample $\boldsymbol{x}$ and is set to 50,000.

4.2 Policy Optimization

We use the P-DQN framework [49] to find the optimal policy π^*. At each time step, the agent takes a hybrid action $a_t \in \mathcal{A}_t$ to perturb the currently modified $\boldsymbol{x}_t$, obtained from the original input $\boldsymbol{x}$. In Q-learning, one aims at finding the optimal Q-value function representing the expected discounted reward for taking action a_t at a given state s_t. Inside the Q-value function, the continuous parameter v_{k_t} is associated with the discrete action k_t, which means v_{k_t} is the optimal action given state s_t and k_t: $v_{k_t} = \arg\sup_v Q(s_{t+1}, k_t, v)$. We therefore cast this as a function $v_{k_t}^Q(s_t)$. Thus, the Bellman equation can be written as:

$$Q(s_t, k_t, v_{k_t}) = \mathbb{E}_{r_t, s_{t+1}}(r_t + \gamma \max_{k_t} Q(s_{t+1}, k_t, v_{k_t}^Q(s_{t+1})) | s_t, a_t = (k_t, v_{k_t})).$$

As with DQN, a deep neural network (DNN) $Q^{\boldsymbol{\theta}_1}(s_t, k_t, v_{k_t})$ is used to approximate the Q-value function, and we fit $v_{k_t}^Q$ with another deterministic policy network $v_{k_t}^{\boldsymbol{\theta}_2}(s_t)$, where $\boldsymbol{\theta}_1$ and $\boldsymbol{\theta}_2$ are the parameters of the two DNNs. To find the optimal $\boldsymbol{\theta}_1^*, \boldsymbol{\theta}_2^*$, we minimize the loss functions below via stochastic gradient descent:

$$\mathcal{L}_Q(\boldsymbol{\theta}_1) = [Q^{\boldsymbol{\theta}_1}(s_t, k_t, v_{k_t}) - y_t]^2, \; \mathcal{L}_\pi(\boldsymbol{\theta}_2) = -\sum_{k_t \in \mathcal{F}} Q(s_t, k_t, v_{k_t}^{\boldsymbol{\theta}_2}(s_t)),$$

where the y_t is the n-step target [38]. Theoretically, as the error diminishes, the Q network converges to the optimal Q-value function and the policy network outputs the optimal continuous action. However, this method is unstable in practice. This is because DQN only samples transition pairs uniformly from the replay buffer. Therefore, we adopt prioritized experience replay [34] to effectively learn from pairs with high expected learning value. As a measurement for learning potential, prioritized experience replay samples transition pairs with probability p_j based on their TD error: $p_t \propto |R_j + \gamma Q_{\text{target}}(s_j, Q(s_j, a_j)) - Q(s_{j-1}, a_{j-1})|^\beta$, where β is a parameter to determine how much prioritization is used. During training, the transition pairs are stored in the replay buffer with their priority; a sum tree data structure is then used to efficiently update the priority and sample pairs from the replay buffer.

4.3 Hierarchical Curiosity-Driven Exploration

In the procedure of generating counterfactual examples, the sparse reward problem is inevitably met due to the large state and action space. Reward shaping is a typical solution that converts the sparse

reward to a dense one [15][11]; however, it is hard to design the intermediate rewards for all black box models. Hence, we develop a hierarchical curiosity-driven exploration mechanism to P-DQN.

Specifically, we adopt a *Random Network Distillation* (RND) module [7], i.e., a curiosity-driven approach to generate state curiosity $r_t^{i,s}$ by quantifying the next-state novelty, which will be further combined with the external rewards r_t to generate the modified reward $r_t' = r_t^{i,s} + r_t$. RND transforms the exploring procedure into a supervised learning task by minimizing the mean squared error:

$$r_t^{i,s} = ||\hat{f}(s_t, \eta_1) - f(s_t)||^2,$$

where $f(s_t)$ is the fixed target network and $\hat{f}(s_t, \eta_1)$ is a trainable predictor network learning to distill the target network. The loss of trained input state (s_t) will decrease as the frequency of visited states increases; therefore, $r_t^{i,s}$ of novel states are expected higher.

Considering that the bonus is obtained after reaching the next state s_{t+1} and will be combined with the environment reward, the agent tends to follow the existing experiences rather than keeps exploring unknown states by taking various actions. To encourage the exploration of different actions at each state, we introduce the RND module to reflect the frequency of each action. At state s_t, the curiosity of a hybrid action $a_t = (k_t, v_{k_t}^{\boldsymbol{\theta}_2}(s_t))$ is given by:

$$r_t^{i,a} = ||\hat{g}(s_t, a_t, \eta_2) - g(s_t, a_t)||^2,$$

where g and $\hat{g}$ have the same role as f and $\hat{f}$, respectively.

Here, we leverage state curiosity $r_t^{i,s}$ to enhance high-level index planning in discrete spaces, and $r_t^{i,a}$ is adopted as low-level action curiosity for enthusiastically searching continuous parameters. Finally, we organically incorporate the two-level curiosity loss into the loss functions defined above in Section 4.2:

$$\mathcal{L}_Q'(\boldsymbol{\theta}_1, \eta_1) = [Q^{\boldsymbol{\theta}_1}(s_t, k_t, v_{k_t}) - y_t]^2 + ||\hat{f}(s_t, \eta_1) - f(s_t)||^2,$$

$$\mathcal{L}_\pi'(\boldsymbol{\theta}_2, \eta_2) = -\sum_{k_t \in \mathcal{F}} Q(s_t, k_t, v_{k_t}^{\boldsymbol{\theta}_2}(s_t)) + ||\hat{g}(s_t, a_t, \eta_2) - g(s_t, a_t)||^2.$$

It is worth remarking that a_t is a function of $\boldsymbol{\theta}_2$. By alternatively updating $\boldsymbol{\theta}_2$ and η_2, the policy network $v_{k_t}^Q$ will learn to balance the action's potential value and novelty.

The overview of our ReLAX framework is depicted in Figure 2.

4.4 Global vs. Local Policy

So far, we have considered one single agent as responsible for generating the CFs for *all* the instances of a given dataset, and hereinafter we refer to it as ReLAX-Global. This allows us to learn a generalized policy that is able to produce counterfactuals, which are not tailored to a specific input sample. Algorithm 1 describes the training of ReLAX-Global with the hierarchical curiosity-driven exploration technique discussed in Section 4.3 above. However, in some cases, the CF generation process should capture the peculiarities of each individual original instance. To accomodate such a need, we introduce a variant called ReLAX-Local.

ReLAX-Local trains a dedicated agent for crafting the optimal CF for a *single* target example. It starts by initializing ReLAX-Local's policy with a pretrained ReLAX-Global's policy. Then, using a standard transfer learning approach [50], ReLAX-Local is fine-tuned on the target samples. This step consists of randomly
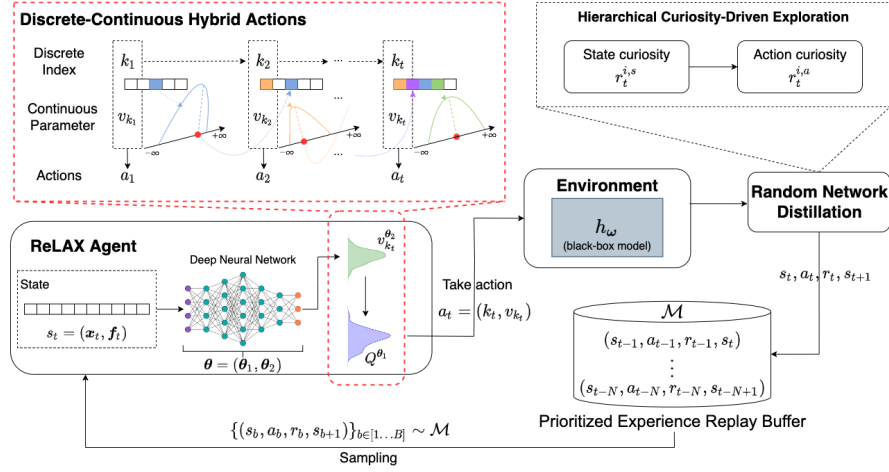
Figure 2: Overview of our proposed ReLAX framework.

Algorithm 1 Training ReLAX-Global Agent with Curiosity

1: $\theta_1 \leftarrow$ *initialize the deep Q-network* Q^{θ_1}
2: $\theta_2 \leftarrow$ *initialize the deterministic policy network* $v_{k_t}^{\theta_2}$
3: $\eta_1 \leftarrow$ *initialize the RND state modules* $\hat{f}, f$
4: $\eta_2 \leftarrow$ *initialize the RND action modules* $\hat{g}, g$
5: $\mathcal{M} \leftarrow$ *initialize the replay buffer*
6: $i \leftarrow 1$
7: **while** $i \leq$ max_epochs **do**
8:     $x \sim \mathcal{D}$ ▷ Sample a training instance x from $\mathcal{D}$
9:     $x_0 \leftarrow x$
10:    $s_0 = (x_0, f_0)$ ▷ Initial state
11:    $t \leftarrow 0$
12:    **for** $t \leq T$ **do** ▷ Maximum agent steps for each sample (T=50,000)
13:       $v_{k_t} \leftarrow v_{k_t}^{\theta_2}(s_t)$ ▷ Compute the continuous parameter
14:       $a_t \leftarrow (k_t, v_{k_t})$ ▷ Select the discrete action by ε-greedy
15:       $r_t^{i,a} \leftarrow ||\hat{g}(s_t, a_t, \eta_2) - g(s_t, a_t)||^2$
16:                   ▷ Generate action curiosity $r_t^{i,a}$
17:       $r_t, s_{t+1} \leftarrow \mathcal{T}(s_t, a_t)$
18:         ▷ The agent gets the reward and observes the next state
19:       $r_t^{i,s} \leftarrow ||\hat{f}(s_t, \eta_1) - f(s_t)||^2, \quad r_t' = r_t^{i,s} + r_t$
20:         ▷ Generate state curiosity $r_t^{i,s}$ and modified reward r_t'
21:       $p_t \leftarrow$ *compute the importance* p_t
22:       $\mathcal{M} \leftarrow (\{s_t\}, \{a_t\}, \{r_t'\}, \{s_{t+1}\}, \{p_t\})$
23:               ▷ Store transition into the replay buffer
24:       $B \sim \mathcal{M}$ ▷ Randomly sample batch B from $\mathcal{M}$
25:       $\theta_1 \leftarrow \theta_1 - \gamma_1 \nabla \mathcal{L}_Q'(\theta_1, \eta_1), \quad \eta_1 \leftarrow \eta_1 - \gamma_2 \nabla \mathcal{L}_Q'(\theta_1, \eta_1)$
26:       $\theta_2 \leftarrow \theta_2 - \gamma_3 \nabla \mathcal{L}_\pi'(\theta_2, \eta_2), \quad \eta_2 \leftarrow \eta_2 - \gamma_4 \nabla \mathcal{L}_\pi'(\theta_2, \eta_2)$
27:           ▷ Update the parameters of both networks via SGD
28:       $t \leftarrow t + 1$
29:    **end for**
30:    $i \leftarrow i + 1$
31: **end while**
32: **return** θ_1, θ_2 ▷ Optimal parameters of both networks

---

generating synthetic training data points around the target example, using a method similar to [13]. Specifically, we uniformly sample data points whose L^2-norm from the target example is at most 1.[3]

---
[3]Notice that all our input samples are normalized unit vectors.

5 EXPERIMENTS

5.1 Setup

Datasets and Tasks. We test with five public tabular datasets described in Table 1, used for classification and regression tasks.

Dataset	N. of Instances	N. of Features	Task
Breast Cancer [5]	699	10 (numerical)	classification
Diabetes [2]	768	8 (numerical)	classification
Sonar [3]	208	60 (numerical)	classification
Wave [4]	5,000	21 (numerical)	classification
Boston Housing [1]	506	14 (mixed)	regression

Table 1: Main characteristics of the five public datasets used.

Predictive Models. Each dataset is randomly split into 70% training and 30% test portions. For each task and the associated dataset, we train the suitable set of predictive models chosen amongst the following: Random Forest (RF), Adaptive Boosting (AdaBoost), Gradient Boosting (XGBoost), Multi-Layer Perceptron (MLP), and Multi-Layer Perceptron for Regression (MLP-Reg). Both MLP and MLP-Reg are fully-connected feed-forward neural networks with two hidden layers; MLP includes also a logistic (i.e., sigmoid) activation function at the last output layer. Notice that some combinations do not apply, e.g., MLP-Reg is only trained on the *Boston Housing* dataset. We perform 10-fold cross validation on the training set portion of each dataset to fine-tune the hyperparameters of all the trainable models. Hence, for each task/dataset pair, we re-train all the applicable models with the best hyperparameters on the whole training set, and we measure their performance on the test set previously hold out. To assess the quality of the predictive models, we use accuracy for classification and RMSE for regression. Eventually, we consider only the best performing model(s) for each task/dataset pair. In Table 2, we summarize the main characteristics of each predictive model used in combination with the benchmarking datasets.
Counterfactual Generator Baselines. We compare ReLAX with all the CF generator baselines described in Section 2. Nearest-CT is considered the simplest approach. Furthermore, we distinguish between *model-specific* and *model-agnostic* methods. The former include: FeatTweak and FOCUS (tree-specific); DeepFool and GRACE (NN-specific). The latter are: LORE, MACE, and DiCE.

Dataset [Best Model]	Structure	Acc. (▲)/RMSE (♦)
Breast Cancer [RF]	{#trees=100}	0.99 (▲)
Diabetes [ADABOOST]	{#trees=100}	0.79 (▲)
Wave [XGBOOST]	{#trees=100}	0.95 (▲)
Breast Cancer [MLP]	{#L1=64, #L2=128}	1.00 (▲)
Sonar [MLP]	{#L1=256, #L2=256}	0.90 (▲)
Wave [MLP]	{#L1=100, #L2=200}	0.97 (▲)
Boston Housing [MLP-REG]	{#L1=50, #L2=128}	3.36 (♦)

Table 2: Model structure and performance for each dataset/task pair.

Methodology. We compare the set of CF generation methods that are suitable for each dataset/target model shown in Table 2. In particular, model-agnostic techniques (including both variants of our ReLAX) clearly apply to every setting, whereas model-specific approaches can be tested only when the target model matches (e.g., FOCUS can be used only in combination with tree-based models). Eventually, we generate a separate CF for each input sample in the test set of every dataset above, using all the CF generators relevant to the setting at hand, i.e., all the model-agnostic methods along with model-specific ones that apply.

Evaluation Metrics. We evaluate the quality of generated CFs according to the following four standard metrics [42]: *Validity*, *Proximity*, *Sparsity*, and *Generation Time*. Validity measures the ratio of CFs that actually meet the prediction goal to the total number of CFs generated:[4] the higher the validity the better. Proximity computes the distance of a CF from the original input sample; in this work, we use L^1-norm to measure proximity, and therefore the smaller it is the better. Sparsity indicates the number of features that must be changed according to a CF, and therefore is equivalent to the L^0-norm between a CF and the corresponding original input sample. The smaller it is the better, as sparser CFs likely lead to more human-interpretable explanations. Finally, Generation Time computes the time required to generate CFs, which, clearly, should be as small as possible. All the metrics above are averaged across all the test input samples. Moreover, experiments were repeated 5 times and results are expressed as the mean ± standard deviation.

5.2 Results

Sparsity-Validity Trade-off. In Figure 3, we plot the number of perturbed features (i.e., sparsity) versus the validity of counterfactuals obtained with different CF generation methods, when applied to classification tasks. More specifically, we fix a threshold on the maximum number of features that each CF generator is allowed to perturb and we show: (*i*) the *actual* sparsity; and (*ii*) the validity of the generated CFs. The rationale of this analysis is to show which method is able to achieve the best trade-off between two contrasting metrics: sparsity and validity. Intuitively, the larger is the number of perturbed features, the higher is the chance of obtaining a valid counterfactual. On the other hand, we should privilege sparser CFs, i.e., CFs that modify as less features as possible, since those are possibly more interpretable and feasible to implement. Results show that both ReLAX-GLOBAL and ReLAX-LOCAL achieve the best balance between sparsity and validity. That is, our method outperforms all the baselines in terms of validity and, more importantly, it obtains these results even when we set a very restrictive threshold on sparsity, i.e., when few features are

---

[4]Some work consider the complementary metric, which is known as *Fidelity* and is equal to (1-*Validity*).

modified. As expected, though, if we soften such a cap on the number of features allowed to change, other methods like LORE may eventually match the performance of ReLAX or even reach higher validity scores. In fact, not controlling for sparsity will make all CF generation methods behave similarly. This is what we observe when we test with DEEPFOOL or the simplest NEAREST-CT baseline, which by design tend to generate valid CFs only if a large fraction of the input features get modified. Due to this behavior, both DEEPFOOL and NEAREST-CT cannot be visualized in the plots, as they fall outside the range of sparsity values imposed in our experiments. Furthermore, although MACE is model-agnostic, its applicability to neural network target models is problematic due to its large computational cost [17]. Besides, the only implementation of MACE remaining available works only in combination with RF target models, and this is why we used it only in the first setting (*Breast Cancer* [RF]).

A similar analysis on the sparsity vs. validity trade-off for the *Boston Housing* regression task is shown in Table 3. In this case, we compare only our two variants of ReLAX since none of the CF generation baselines considered is designed to operate in a regression setting. As expected, the larger is the tolerance δ used to determine if the prediction goal of the counterfactual example is met the harder is for ReLAX to find a valid counterfactual.

	Validity (Sparsity)	
Threshold (δ)	RELAX-GLOBAL	RELAX-LOCAL
0.20	0.81 ± 0.09 (3.02 ± 0.17)	**0.87 ± 0.05 (3.10 ± 0.18)**
0.40	0.74 ± 0.06 (3.09 ± 0.16)	**0.81 ± 0.05 (3.18 ± 0.16)**
0.60	0.70 ± 0.06 (3.21 ± 0.12)	**0.77 ± 0.03 (3.28 ± 0.09)**

Table 3: *Sparsity* vs. *Validity* of counterfactuals generated by ReLAX for the *Boston Housing* regression task.

Finally, analogous conclusions can be drawn if we compare proximity vs. validity (see Table 4): ReLAX is able to strike the best balance also between those two conflicting metrics.

Generation Time. Although validity and sparsity (proximity) are crucial to measure the quality of a CF generation method, efficiency is pivotal as well. Therefore, we compare the average generation time for each model-agnostic CF generator, namely LORE, MACE, and our ReLAX in its two variants. We focus on model-agnostic methods because we want this comparison to be as general as possible. Table 4 shows that our method takes up to 42% less time than other model-agnostic baseline to produce valid counterfactuals, which happen to be also closer to the original instances. This result is even more remarkable if we consider that the counterfactual generation time of ReLAX includes the training of the DRL agent.

5.3 Hyperparameter Tuning

Our CF generation method is associated with a number of controlling parameters. To understand the impact of these parameters, we analyze the behavior of ReLAX on the *Sonar* dataset with MLP as the target classifier and the maximal sparsity limited to 5 features.

The scaling factor λ. We first investigate the effect of the scaling factor λ on the generated CFs, picking it from 0.001, 0.01, 0.1, 1, 10. As shown in Figure 4, λ controls the balance between sparsity and validity. Indeed, larger values of λ force the agent to prefer sparser CFs at the expense of lower validity (see Figure 4 – left), whereas smaller values of λ result in the opposite (see Figure 4 – right).
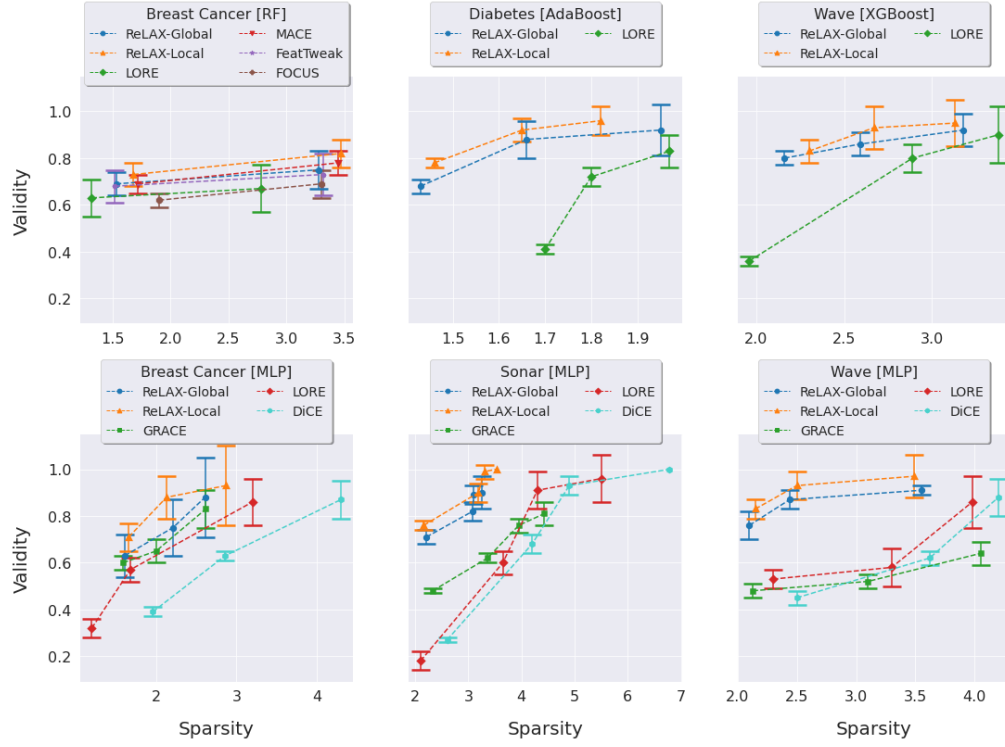
Figure 3: *Sparsity* vs. *Validity* of counterfactuals generated by RELAX and other baselines for classification tasks.

Metric	Dataset [Models]	CF Generation Methods			
		RELAX-GLOBAL	RELAX-LOCAL	LORE	MACE
Proximity	*Breast Cancer* [RF, MLP]	[**4.46**, 5.92]	[4.49, 5.87]	[4.63, **5.63**]	[4.47, N/A]
	Diabetes [ADABOOST]	[**4.41**]	[4.50]	[4.76]	[N/A]
	Sonar [MLP]	[**7.32**]	[7.66]	[7.36]	[N/A]
	Wave [XGBOOST, MLP]	[**5.93, 6.38**]	[6.02, 6.50]	[6.60, 6.41]	[N/A, N/A]
	Boston Housing [MLP-REG]	[**5.10**]	[5.36]	[N/A]	[N/A]
Generation Time (secs.)	*	1500	**1320**	2100	2280

Table 4: Comparison of *Proximity* and *Generation Time* for model-agnostic CF generation methods.
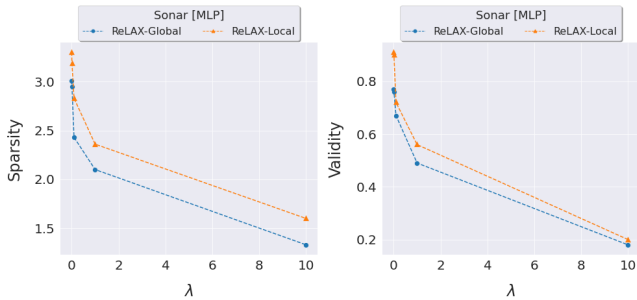
Figure 4: The effect of λ on *Sparsity* (left) and *Validity* (right).

The target model's architecture. We assess the robustness of our CF generation method when applied to different target neural network architectures. More specifically, Table 5 shows the impact of different MLP architectures on the validity and sparsity of counterfactuals generated by RELAX in comparison with two competitors: GRACE (NN-specific) and LORE (model-agnostic). We may observe that both GRACE and LORE are quite sensitive to the MLP size, i.e., when the target neural network is getting large the validity

		Validity (Sparsity)			
MLP size	Acc.	RELAX-GLOBAL	RELAX-LOCAL	GRACE	LORE
[256, 256]	0.88	0.76 (**2.95**)	**0.90** (3.19)	0.62 (3.32)	0.60 (3.65)
[128, 128]	0.85	0.80 (**2.69**)	**0.90** (2.88)	0.73 (2.85)	0.76 (3.21)
[64, 64]	0.79	0.90 (**1.88**)	**0.95** (1.93)	0.86 (1.90)	0.90 (2.52)

Table 5: The impact of different MLP architectures on the *Validity* (*Sparsity*) of counterfactuals.

and sparsity of CFs generated with those two methods deteriorate significantly. In the case of GRACE, the reason for that detrimental effect is due to the fact that it leverages the gradient of the function approximated by the neural network, which is obviously correlated with the complexity of the MLP structure. Despite model-agnostic, LORE requires to accurately learn a locally-interpretable surrogate model of the target neural network, which may be hard when this becomes too complex. Instead, RELAX is more robust toward different MLP structures, and its performance is consistent independently of the MLP size. Indeed, the agent underneath RELAX *truly* treats the target model as a black box regardless of its internal complexity. ***The efficiency of pretraining.*** Finally, we show how pretrained RELAX-GLOBAL improves the performance of RELAX-LOCAL. More specifically, we train RELAX-LOCAL as described in Section 4.4, and

compare it with another agent learned from scratch. Unsurprisingly, initializing ReLAX-Local with pretrained ReLAX-Global reduces its CFs generation time, as shown in Table 6.

Setting	Validity (Sparsity)	Gen. Time (secs.)
without pretraining	0.80 (3.27)	1132
with pretraining	**0.90 (3.19)**	**500**

Table 6: Performance of ReLAX-Local **with/without pretrained** ReLAX-Global**.**

6 CASE STUDY: COVID-19 MORTALITY

The goal of this case study is to demonstrate that counterfactual explanations provided by ReLAX may help countries that suffer from high COVID-19 mortality taking effective actions, economically and medically, to reduce such risk.

To achieve that, we first need to learn a binary classifier that predicts whether the country's death risk due to COVID-19 is high or not, given the country-level features. Inspired by previous work addressing a similar task [6], we gather 17 country-level demographic features from 156 countries across 7 continents [8, 46–48]. Furthermore, we label each instance with a binary class denoting the COVID-19 risk of mortality ("high" vs. "normal"), as in [6]. This dataset is made publicly available.[5]

We randomly split our collected dataset into two parts, i.e., 70% used for training and 30% for test. Therefore, we train the following models to learn the binary classifier for predicting COVID-19 mortality risk: SVM, RF, AdaBoost, and XGBoost. After running 10-fold cross validation, the best-performing model turns out to be XGBoost with 500 trees, which achieves 85% accuracy on the test set. We sort the features according to the ranking induced by the XGBoost model, as shown in Figure 5 (left). Then, we generate with our ReLAX algorithm the CFs for the 16 high-risk countries in the test set. It is worth remarking that, although the target binary classifier is learned considering *all* the features from the whole training set, we force ReLAX to tweak only the subset of *actionable* features so that effective suggestions can be found by observing the generated CFs. Besides, in order to avoid bizarre recommendations, we constrain the change of (actionable) features toward a "plausible" direction (e.g., it would not make any sense to suggest increasing the unemployment rate of a country).

The ReLAX agent tweaks 1.67 features on average, and the average proximity (i.e., L^1-norm) between the original sample and the corresponding counterfactual example is 1.18. Figure 5 (right) shows the direction of feature changes as suggested by the CFs.

We observe that the CFs suggest five main changes: *(i)* Decreasing the death rate;[6] *(ii)* Decreasing the unemployment rate; *(iii)* Increasing the nurse rate per 10,000 people; *(iv)* Decreasing the urban population rate; and *(v)* Decreasing the obesity prevalence. Not only those recommendations look sensible, as much as straightforward or even obvious, but their accuracy is also confirmed by the fact that many countries have indeed adopted similar strategies to counter the impact of COVID-19. For example, US approved the visa for more than 5,000 international nurses to strengthen the health

workforce.[7] Moreover, according to the investigation made by the US Center for Disease Control and Prevention,[8] obese patients with COVID-19 aged 18 years and younger are associated with a 3.07 times higher risk of hospitalization and a 1.42 times higher risk of severe illness. Thus, reducing the obesity prevalence can indeed lower mortality risk. Finally, reducing the unemployment rate and the urban population rate may allow a broader range of people to enhance their social community awareness, take consciousness of the risks of the pandemic, and thus adopt a safe lifestyle.
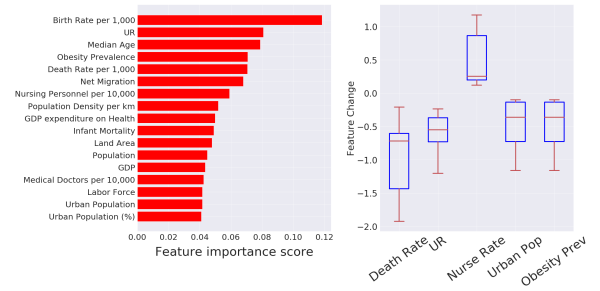

Figure 5: Left: Ranking of feature importance. Right: Suggested feature changes for lowering high mortality risk.

7 CONCLUSION AND FUTURE WORK

In this work, we presented ReLAX, the first method for generating model-agnostic counterfactual examples based on deep reinforcement learning with hierarchical curiosity-driven exploration. We implemented two variants of it: ReLAX-Global and ReLAX-Local. The former learns a generalized agent's policy from a whole set of training instances, whereas the latter trains a dedicated agent's policy for crafting the optimal counterfactual of a single target example via transfer learning from a pretrained ReLAX-Global. Extensive experiments run on five public tabular datasets demonstrated that ReLAX significantly outperforms all the considered CF generation baselines in every standard quality metric. Our method is scalable with respect to the number of features and instances, and can explain *any* black-box model, regardless of its internal complexity and prediction task (i.e., classification or regression). Finally, we show that CFs generated by ReLAX are useful in practice, as they can be used to suggest actions that a country should take to reduce the risk of COVID-19 mortality.

Several research directions are worth exploring in future work. For example: extend ReLAX to generate explanations for non-tabular input data like images, and compare our method against non-counterfactual explanation approaches like SHAP [24] or LIME [31].

---

[5]https://github.com/Mewtwo1996/ReLAX.git
[6]Albeit it may sound odd, reducing the death rate can subsume a broader suggestion for improving the life quality of a country.

[7]https://www.npr.org/sections/health-shots/2022/01/06/1069369625/short-staffed-and-covid-battered-u-s-hospitals-are-hiring-more-foreign-nurses
[8]https://www.cdc.gov/obesity/data/obesity-and-covid-19.html

REFERENCES

[1] 1978. Boston Housing Dataset. [Online]. Available from: https://www.kaggle.com/vikrishnan/boston-house-prices.

[2] 1988. Diabetes Dataset. [Online]. Available from: https://www.kaggle.com/uciml/pima-indians-diabetes-database.

[3] 1988. Sonar Dataset. [Online]. Available from: https://archive.ics.uci.edu/ml/datasets/connectionist+bench+(sonar,+mines+vs.+rocks).

[4] 1988. Wave Dataset. [Online]. Available from: https://archive.ics.uci.edu/ml/datasets/waveform+database+generator+(version+1).

[5] 1995. Breast Cancer Dataset. [Online]. Available from: https://archive.ics.uci.edu/ml/datasets/breast+cancer+wisconsin+(diagnostic).

[6] Jordan J. Bird, Chloe M. Barnes, Cristiano Premebida, Anikó Ekárt, and Diego R. Faria. 2020. Country-level Pandemic Risk and Preparedness Classification based on COVID-19 Data: A Machine Learning Approach. *PLoS One* 15, 10 (2020).

[7] Yuri Burda, Harrison Edwards, Amos Storkey, and Oleg Klimov. 2018. Exploration by Random Network Distillation. *arXiv preprint arXiv:1810.12894* (2018).

[8] Central Intelligency Agency. 2020. The CIA World Factbook2020.

[9] Susanne Dandl, Christoph Molnar, Martin Binder, and Bernd Bischl. 2020. Multi-Objective Counterfactual Explanations. In *Proc. of PPSN (Lecture Notes in Computer Science, Vol. 12269)*, Thomas Bäck, Mike Preuss, André H. Deutz, Hao Wang, Carola Doerr, Michael T. M. Emmerich, and Heike Trautmann (Eds.). Springer, 448–469. https://doi.org/10.1007/978-3-030-58112-1_31

[10] EU. 2016. Regulation (EU) 2016/679 of the European Parliament (GDPR). *Official Journal of the European Union* L119 (2016), 1–88.

[11] Marek Grzes and Daniel Kudenko. 2009. Theoretical and Empirical Analysis of Reward Shaping in Reinforcement Learning. In *2009 International Conference on Machine Learning and Applications*. IEEE, 337–344.

[12] Riccardo Guidotti. 2022. Counterfactual Explanations and How to Find Them: Literature Review and Benchmarking. *Data Mining and Knowledge Discovery* (2022), 1–55.

[13] Riccardo Guidotti, Anna Monreale, Salvatore Ruggieri, Dino Pedreschi, Franco Turini, and Fosca Giannotti. 2018. Local Rule-Based Explanations of Black Box Decision Systems. *arXiv preprint arXiv:1805.10820* (2018).

[14] Matthew Hausknecht, Prannoy Mupparaju, Sandeep Subramanian, Shivaram Kalyanakrishnan, and Peter Stone. 2016. Half Field Offense: An Environment for Multiagent Learning and Ad Hoc Teamwork. In *Proc. of ALA Workshop*.

[15] Yujing Hu, Weixun Wang, Hangtian Jia, Yixiang Wang, Yingfeng Chen, Jianye Hao, Feng Wu, and Changjie Fan. 2020. Learning to Utilize Shaping Rewards: A New Approach of Reward Shaping. *Advances in Neural Information Processing Systems* 33 (2020), 15931–15941.

[16] Kentaro Kanamori, Takuya Takagi, Ken Kobayashi, and Hiroki Arimura. 2020. DACE: Distribution-Aware Counterfactual Explanation by Mixed-Integer Linear Optimization. In *Proc. of IJCAI*, Christian Bessiere (Ed.). ijcai.org, 2855–2862. https://doi.org/10.24963/ijcai.2020/395

[17] Amir-Hossein Karimi, Gilles Barthe, Borja Balle, and Isabel Valera. 2020. Model-Agnostic Counterfactual Explanations for Consequential Decisions. In *Proc. of AISTATS*, Silvia Chiappa and Roberto Calandra (Eds.), Vol. 108. PMLR, 895–905. http://proceedings.mlr.press/v108/karimi20a.html

[18] Amir-Hossein Karimi, Bodo Julius von Kügelgen, Bernhard Schölkopf, and Isabel Valera. 2020. Algorithmic Recourse Under Imperfect Causal Knowledge: A Probabilistic Approach. In *Proc. of NeurIPS (NeurIPS'20)*, Hugo Larochelle, Marc'Aurelio Ranzato, Raia Hadsell, Maria-Florina Balcan, and Hsuan-Tien Lin (Eds.). https://proceedings.neurips.cc/paper/2020/hash/02a3c7fb3f489288ae6942498498db20-Abstract.html

[19] Mehdi Khamassi, George Velentzas, Theodore Tsitsimis, and Costas Tzafestas. 2017. Active Exploration and Parameterized Reinforcement Learning Applied to a Simulated Human-Robot Interaction Task. In *2017 First IEEE International Conference on Robotic Computing (IRC)*. IEEE, 28–35.

[20] Thai Le, Suhang Wang, and Dongwon Lee. 2020. GRACE: Generating Concise and Informative Contrastive Sample to Explain Neural Network Model's Prediction. In *Proc. of KDD (KDD'20)*, Rajesh Gupta, Yan Liu, Jiliang Tang, and B. Aditya Prakash (Eds.). ACM, 238–248.

[21] Timothy P. Lillicrap, Jonathan J. Hunt, Alexander Pritzel, Nicolas Heess, Tom Erez, Yuval Tassa, David Silver, and Daan Wierstra. 2016. Continuous Control with Deep Reinforcement Learning. In *Proc. of ICLR (ICLR'16)*, Yoshua Bengio and Yann LeCun (Eds.). http://arxiv.org/abs/1509.02971

[22] Ana Lucic, Harrie Oosterhuis, Hinda Haned, and Maarten de Rijke. 2022. FOCUS: Flexible Optimizable Counterfactual Explanations for Tree Ensembles. In *Proc. of AAAI (AAAI'22)*. 5313–5322. https://doi.org/10.1609/aaai.v36i5.20468

[23] Ana Lucic, Maartje A. Ter Hoeve, Gabriele Tolomei, Maarten De Rijke, and Fabrizio Silvestri. 2022. CF-GNNExplainer: Counterfactual Explanations for Graph Neural Networks. In *Proc. of AISTATS (AISTATS'22, Vol. 151)*, Gustau Camps-Valls, Francisco J. R. Ruiz, and Isabel Valera (Eds.). PMLR, 4499–4511. https://proceedings.mlr.press/v151/lucic22a.html

[24] Scott M Lundberg and Su-In Lee. 2017. A Unified Approach to Interpreting Model Predictions. In *Advances in Neural Information Processing Systems 30*, I. Guyon, U. V. Luxburg, S. Bengio, H. Wallach, R. Fergus, S. Vishwanathan, and R. Garnett (Eds.). Curran Associates, Inc., 4765–4774. http://papers.nips.cc/paper/7062-a-unified-approach-to-interpreting-model-predictions.pdf

[25] Warwick Masson, Pravesh Ranchod, and George Konidaris. 2016. Reinforcement Learning with Parameterized Actions. In *Proc. of AAAI (AAAI'16)*. AAAI Press, 1934–1940.

[26] Volodymyr Mnih, Koray Kavukcuoglu, David Silver, Alex Graves, Ioannis Antonoglou, Daan Wierstra, and Martin Riedmiller. 2013. Playing Atari with Deep Reinforcement Learning. In *NIPS Deep Learning Workshop*.

[27] Seyed-Mohsen Moosavi-Dezfooli, Alhussein Fawzi, and Pascal Frossard. 2016. DeepFool: A Simple and Accurate Method to Fool Deep Neural Networks. In *Proc. of CVPR (CVPR'16)*. IEEE Computer Society, 2574–2582. https://doi.org/10.1109/CVPR.2016.282

[28] Ramaravind Kommiya Mothilal, Amit Sharma, and Chenhao Tan. 2020. Explaining Machine Learning Classifiers through Diverse Counterfactual Explanations. In *Proc. of FAT* (FAT*'20)*, Mireille Hildebrandt, Carlos Castillo, L. Elisa Celis, Salvatore Ruggieri, Linnet Taylor, and Gabriela Zanfir-Fortuna (Eds.). ACM, 607–617. https://doi.org/10.1145/3351095.3372850

[29] Martin Pawelczyk, Klaus Broelemann, and Gjergji Kasneci. 2020. Learning Model-Agnostic Counterfactual Explanations for Tabular Data. In *Proc. of WWW (TheWebConf'20)*, Yennun Huang, Irwin King, Tie-Yan Liu, and Maarten van Steen (Eds.). ACM / IW3C2, 3126–3132. https://doi.org/10.1145/3366423.3380087

[30] Rafael Poyiadzi, Kacper Sokol, Raul Santos-Rodriguez, Tijl De Bie, and Peter Flach. 2020. FACE: Feasible and Actionable Counterfactual Explanations. In *Proc. of AIES (AIES'20)*. 344–350.

[31] Marco Tulio Ribeiro, Sameer Singh, and Carlos Guestrin. 2016. "Why Should I Trust You?": Explaining the Predictions of Any Classifier. In *Proc. of KDD (KDD'16)*. ACM, 1135–1144. https://doi.org/10.1145/2939672.2939778

[32] Chris Russell. 2019. Efficient Search for Diverse Coherent Explanations. In *Proc. of FAT* (FAT*'19)*, Danah Boyd and Jamie H. Morgenstern (Eds.). ACM, 20–28. https://doi.org/10.1145/3287560.3287569

[33] Wojciech Samek, Grégoire Montavon, Andrea Vedaldi, Lars Kai Hansen, and Klaus-Robert Müller. 2019. *Explainable AI: Interpreting, Explaining and Visualizing Deep Learning*. Springer.

[34] Tom Schaul, John Quan, Ioannis Antonoglou, and David Silver. 2015. Prioritized Experience Replay. *arXiv preprint arXiv:1511.05952* (2015).

[35] Alexander A Sherstov and Peter Stone. 2005. Function Approximation via Tile Coding: Automating Parameter Choice. In *International Symposium on Abstraction, Reformulation, and Approximation*. Springer, 194–205.

[36] Thomas Spooner, Danial Dervovic, Jason Long, Jon Shepard, Jiahao Chen, and Daniele Magazzeni. 2021. Counterfactual Explanations for Arbitrary Regression Models. *CoRR* abs/2106.15212 (2021). https://arxiv.org/abs/2106.15212

[37] Ilia Stepin, Jose M Alonso, Alejandro Catala, and Martín Pereira-Fariña. 2021. A Survey of Contrastive and Counterfactual Explanation Generation Methods for Explainable Artificial Intelligence. *IEEE Access* 9 (2021), 11974–12001.

[38] Richard S. Sutton and Andrew G. Barto. 1998. *Reinforcement Learning: An Introduction*. MIT Press. http://www.cs.ualberta.ca/~sutton/book/the-book.html

[39] Gabriele Tolomei and Fabrizio Silvestri. 2021. Generating Actionable Interpretations from Ensembles of Decision Trees. *IEEE Transactions on Knowledge and Data Engineering* 33, 4 (2021), 1540–1553. https://doi.org/10.1109/TKDE.2019.2945326

[40] Gabriele Tolomei, Fabrizio Silvestri, Andrew Haines, and Mounia Lalmas. 2017. Interpretable Predictions of Tree-based Ensembles via Actionable Feature Tweaking. In *Proc. of KDD (KDD'17)*. ACM, 465–474. https://doi.org/10.1145/3097983.3098039

[41] Berk Ustun, Alexander Spangher, and Yang Liu. 2019. Actionable Recourse in Linear Classification. In *Proc. of FAT* (FAT*'19)*, Danah Boyd and Jamie H. Morgenstern (Eds.). ACM, 10–19. https://doi.org/10.1145/3287560.3287566

[42] Sahil Verma, John Dickerson, and Keegan Hines. 2020. Counterfactual Explanations for Machine Learning: A Review. *arXiv preprint arXiv:2010.10596* (2020).

[43] Sandra Wachter, Brent Mittelstadt, and Chris Russell. 2017. Counterfactual Explanations without Opening the Black Box: Automated Decisions and the GDPR. *Harvart Journal of Law & Tech.* 31 (2017), 841.

[44] Yongjie Wang, Qinxu Ding, Ke Wang, Yue Liu, Xingyu Wu, Jinglong Wang, Yong Liu, and Chunyan Miao. 2021. The Skyline of Counterfactual Explanations for Machine Learning Decision Models. In *Proc. of CIKM (CIKM'21)*. ACM, 2030–2039.

[45] Ermo Wei, Drew Wicke, and Sean Luke. 2018. Hierarchical Approaches for Reinforcement Learning in Parameterized Action Space. In *2018 AAAI Spring Symposium Series*.

[46] World Health Organization. 2017. Prevalence of Obesity among Adults.

[47] World Health Organization. 2020. Global Health Workforce Statistics.

[48] Worldometers. 2013. Current World Population.

[49] Jiechao Xiong, Qing Wang, Zhuoran Yang, Peng Sun, Lei Han, Yang Zheng, Haobo Fu, Tong Zhang, Ji Liu, and Han Liu. 2018. Parametrized Deep Q-networks Learning: Reinforcement Learning with Discrete-Continuous Hybrid Action Space. *arXiv preprint arXiv:1810.06394* (2018).

[50] Fuzhen Zhuang, Zhiyuan Qi, Keyu Duan, Dongbo Xi, Yongchun Zhu, Hengshu Zhu, Hui Xiong, and Qing He. 2021. A Comprehensive Survey on Transfer Learning. *Proc. IEEE* 109, 1 (2021), 43–76. https://doi.org/10.1109/JPROC.2020.3004555